Research Article

PSUN: An OFDM-Pulsed Radar Coexistence Technique with Application to 3.5 GHz LTE

Seungmo Kim, Junsung Choi, and Carl Dietrich

Bradley Department of Electrical and Computer Engineering, Virginia Tech, Blacksburg, VA 24060, USA

Correspondence should be addressed to Seungmo Kim; seungmo@vt.edu

Received 3 March 2016; Accepted 3 May 2016

Academic Editor: Miguel López-Benítez

This paper proposes Precoded SUbcarrier Nulling (PSUN), an orthogonal frequency-division multiplexing (OFDM) transmission strategy for a wireless communications system that needs to coexist with federal military radars generating pulsed signals in the 3.5 GHz band. This paper considers existence of Environmental Sensing Capability (ESC), a sensing functionality of the 3.5 GHz band coexistence architecture, which is one of the latest suggestions among stakeholders discussing the 3.5 GHz band. Hence, this paper considers impacts of imperfect sensing for a precise analysis. Imperfect sensing occurs due to either a sensing error by an ESC or a parameter change by a radar. This paper provides a framework that analyzes performance of an OFDM system applying PSUN with imperfect sensing. Our results show that PSUN is still effective in suppressing ICI caused by radar interference even with imperfect pulse prediction. As an example application, PSUN enables LTE downlink to support various use cases of 5G in the 3.5 GHz band.

1. Introduction

In 2010, the US National Telecommunications and Information Administration (NTIA) Fast Track Report [1] identified the 3550–3650 MHz band to be potentially suitable for commercial broadband use. The NTIA identified it as one of the candidate bands, in response to the president's initiative [2] to identify 500 megahertz of spectrum for commercial wireless broadband. In 2012, the Federal Communications Commission (FCC) released a Notice of Proposed Rulemaking (NPRM) [3] where they proposed creation of the Citizens Broadband Radio Service (CBRS). The FCC voted to approve the suggestions developed through two NPRMs [3, 4] and adopted rules for managing 150 megahertz in the 3550–3700 MHz band (the 3.5 GHz band) in a report and order [5].

The FCC proposes structuring the CBRS according to a *three-tiered* shared access model comprised of Incumbent Access (IA), Priority Access (PA), and General Authorized Access (GAA). IA includes federal military radars and fixed satellite service, which are protected from PA and GAA. PA operations are protected from GAA operations. Priority Access License (PAL), three-year authorization to use a 10-megahertz channel in a single census tract, will be assigned in up to 70 megahertz of the 3550–3650 MHz portion of the band. GAA use will be allowed throughout the 150-megahertz band. GAA users will receive no protection from interference of other CBRS users. There exist *spectrum access systems (SASs)* incorporating a dynamic database and interference mitigation techniques. A SAS collects pulse parameters of the incumbent radars and provides them with the coexisting CBRS devices. In many cases, a SAS may not be able to provide such information directly to the CBRS users due to security concerns related to military radar systems. Then, a SAS provides such information in an indirect manner, for example, query responses to the CBRS users.

The NTIA recommends addition of Environmental Sensing Capability (ESC), a component for *sensing capability* [6]. The NTIA's review of the public record indicates that many stakeholders proposed employing sensing techniques to augment capability of a SAS. The inputs from the ESC can be used by the SAS to direct the PA and GAA tier users to another channel or, if necessary, to cease transmissions to avoid potential harmful interference to federal radar systems.

In addition, the FCC recommends in [3, 4] the CBRS system to be a small-cell system where each transmitter can keep its transmitting power low. The most popular examples

of small-cell systems so far in practice are Wireless Fidelity (Wi-Fi) and the 3rd Generation Partnership Project (3GPP) Long-Term Evolution (LTE). To the best of our knowledge, it is more challenging to design a small-cell system based on LTE (than Wi-Fi) because as a "cellular" system it tends to have higher requirements, for example, higher mobility with lower latency. Therefore, we set LTE as our model system for the CBRS in the 3.5 GHz band. Contributions of this paper are summarized as follows.

(1) This paper proposes Precoded SUbcarrier Nulling (PSUN), an OFDM transmission strategy that effectively suppresses pulsed interference from a radar. By applying PSUN at a transmitter (Tx) and pulse blanking (PB) at a receiver (Rx), an LTE system can mitigate intercarrier interference (ICI) caused by pulsed interference from coexisting radars. It is noteworthy that this paper suggests a coexistence method *without modifying the incumbent radars' operations*.

(2) This paper provides an analysis framework for OFDM-pulsed radar coexistence. To the best of our knowledge, this paper is the first work that considers existence of ESC in the coexistence problem, which reflects uniqueness of the problem that it is managed by both means of database and spectrum sensing. Furthermore, the framework takes into account the impacts of *imperfect prediction of radar interference*.

(3) This paper suggests use cases of the fifth-generation (5G) mobile networks that LTE downlink can support by using the 3.5 GHz band, based on the analyses and results that this paper provides.

2. Related Work

In [7], a novel radar waveform that minimizes a radar's in-band interference on a coexisting communications system is proposed. This approach assumes that a radar has full knowledge of the interference channel and modifies its own signal vectors in such a way that they fall into the null space of the channel matrix between the radar and the coexisting communications system. In [8], the coexistence scenario of [7] is extended to more than one interference channel. Our work is distinguished from [7, 8] because it proposes a strategy that requires *no change of the incumbent radar system*. It is a meaningful contribution considering the widely acknowledged concern about national security and cost of changing the incumbent system.

In [9, 10], opportunistic spectrum sharing between an incumbent radar and a secondary cellular system is studied. The work specifies applications that are feasible in such a coexistence scenario. It is found that noninteractive video on demand, peer-to-peer file sharing, file transfers, automatic meter reading, and web browsing are feasible, while real-time transfers of small files and VoIP are not. In [11], it is suggested that the secondary communication system utilizes information of the incumbent radar that is provided by a database. In [12], impacts of interference from shipborne radars to LTE systems are studied. An eNodeB's signal-to-interference-plus-noise ratio (SINR) plummets when hit by radar pulses, but an LTE system is able to recover during the time between radar pulses. Average throughput of user equipment (UE) drops under radar interference. The authors concluded that the UE throughput loss in the uplink direction is tolerable even with a radar deployed only 50 kilometers away from the LTE system. In [13], the study in [12] is extended. The authors studied impacts of shipborne radars that operate in the same channel and are located in the vicinity of a 3.5 GHz macrocell and outdoor small-cell LTE systems. With such additional consideration of out-of-band effects of shipborne radars, the authors still conclude that both macrocell and outdoor small-cell LTE systems can operate inside current exclusion zones. In [14], on the other hand, it is concluded that LTE systems are unable to cope well with narrowband bursty interference on the downlink. Our work is distinguished from [9–14] because this paper studies *how to actually cancel radar interference*, while only feasibility of coexistence was discussed in the prior studies.

In addition, this paper provides *a generalized analytical framework*. This paper takes into consideration a comprehensive interplay among multiple variables regarding the military radars' operations, such as the number of radars, pulse parameters, antenna sidelobes, and out-of-band emissions, which will be discussed in Section 3. Moreover, impacts of imperfect prediction of radar interference are measured by appropriate probabilities which will be explained in Section 5.

Note that this paper is an extension of our previous study that was published in [15]. The extension is twofold: (i) we change the performance metric from bit error rate to maximum data rate to more fairly reflect the impact of PSUN on an OFDM system performance; (ii) we use 3.5 GHz LTE as a near-term example that serves to illustrate how the technique could be applied to operation of future 5G systems in bands shared with pulsed radars.

3. Coexistence Model

This paper discusses the performance of an LTE small-cell system that coexists with multiple military radars that rotate and generate pulsed signals. Note that this paper focuses on the *downlink* of an LTE system where an eNodeB acts as a Tx and a UE becomes an Rx.

Also, this paper assumes that there is no impact of fading from mobility nor multipath since the ICI that is caused by radar interference has far more significant impacts than Doppler shift and delay spread. Therefore, we assume that the only two channel impairments are *radar interference* and *additive white Gaussian nose (AWGN)*. In other words, an OFDM symbol goes through an AWGN channel when the LTE system is not interfered by the radar. There is a period of time when the radar beam does not point at the LTE system since a radar rotates; during this time, an LTE system is assumed to experience an AWGN channel. It should be noted that hence the simulation results that are presented in Section 6 do not take fading into consideration.

3.1. Characterization of a Military Radar. It is very important to note that a 3.5 GHz band coexistence problem is more challenging than what is often acknowledged. This paper

Table 1: Parameters for antenna horizontal sidelobe analysis.

Parameter	Remark
θ_{beam}	Angle of a radar antenna's horizontal beam with main lobe and sidelobes that cause interference on an LTE system
θ_{pass}	Angle that a radar antenna's horizontal beam passes through an LTE cell
θ_{intf}	The total angle that a radar antenna's horizontal beam interferes with an LTE cell
d	Distance between a radar and an LTE cell
r_c	Diameter of an LTE cell
T_{rot}	Radar rotation time

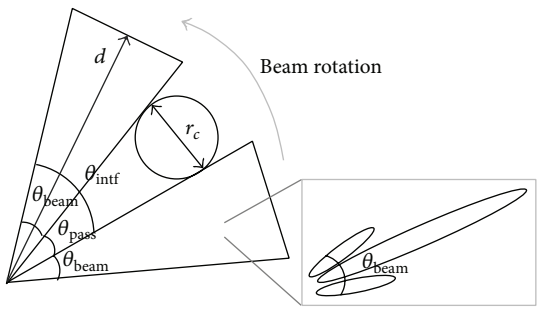

Figure 1: Impact of antenna horizontal sidelobes.

considers two aspects that increase the impact of a pulsed radar's interference on an LTE cell: a radar's antenna sidelobes and out-of-band emissions. These analogous spatial and frequency domain effects are serious due to the *extreme difference in transmitting power between radar and LTE*.

3.1.1. Antenna Sidelobes. Following the FCC's guideline in designing a CBRS system coexisting with military radars [3–5], a sufficiently large spatial separation must be guaranteed between a federal military radar and an LTE system to guarantee a low level of interference from an LTE eNodeB (Tx) to the radar. In spite of this large distance from a radar, an LTE UE (Rx) cannot avoid radar interference with a very high level due to the much higher transmitting power of a radar. The power of a radar's signal received at an LTE Rx is so high that even sidelobes cause significant interference to the communications system. This is interpreted as *a greater value of horizontal angle of a radar's beam* that actually causes interference on a coexisting LTE system. Figure 1 illustrates such an impact of a radar antenna's horizontal sidelobes. It describes that the angle of a radar beam, θ_{beam}, contains not only its main lobe but also the sidelobes. The value of θ_{beam} differs according to type of radar. For instance, the antenna pattern of a radar analyzed in [1] has cosine pattern with sidelobes that are 14.4 dB lower than the main lobe.

Now we formulate such a coexistence model in which an LTE system is interfered by a radar that rotates and transmits pulses. Table 1 describes parameters used in the analysis, including those shown in Figure 1. Suppose that a radar rotates counterclockwise and an LTE system is within interference range of the radar's signal. The angle of rotation during which the radar's beam passes through a cell of an LTE system is given by

$$\theta_{\text{pass}} = \frac{360^\circ \cdot r_c}{2\pi d}. \tag{1}$$

As illustrated in Figure 1, the total angle through which the radar beam interferes with a cell of an LTE system can be written as

$$\theta_{\text{intf}} = \theta_{\text{beam}} + \theta_{\text{pass}}. \tag{2}$$

Note that θ_{beam} differs according to type of radar, while θ_{pass} is determined by d and r_c. Then the total interference time is defined as the time period when a cell of an LTE system is interfered by a radar within a beam rotation, which is obtained by

$$T_{\text{intf}} = \frac{\theta_{\text{intf}}}{360} \cdot T_{\text{rot}}. \tag{3}$$

Such an impact of a radar's antenna horizontal sidelobes is evidenced in Figure 5 of [16]. The report describes an observed case in which a wireless communication system receives energy from an SPN-43 shipborne radar at a level that is approximately 30 dB higher than the noise floor, even when the main lobe of the radar antenna is towards the direction opposite to a cell of the wireless communications system. This implies that sidelobes of a radar beam can have a significant impact on operation of a coexisting wireless communications system.

3.1.2. Out-of-Band Emission. Due to extremely high peak transmitting power of a radar, out-of-band emission from a radar operating in a neighboring channel also has a significant impact on a coexisting LTE system. Radars themselves are separated among different channels to avoid interfering with each other. This spectral separation is enough to protect radars from interference due to other radars but is insufficient to protect a wireless communications system that operates with a much lower transmitting power.

Figure 2 illustrates a simulation result of a radar's out-of-band interference on an LTE system. We simulated an LTE system operating at 3.5 GHz and a radar generating pulses at 3.5, 3.55, and 3.6 GHz. The transmitting powers of a radar and an LTE eNodeB are assumed to be 83 dBm and 23 dBm, respectively. The distance between an LTE eNodeB and a UE is 100 meters, while the radar is assumed to be separated by distance of 100 kilometers. Also, the radar's pulse repetition time (PRT) and duty cycle are 1 msec and 10%, respectively. A radar has an extremely large bandwidth due to its pulsed nature. Since transmitting power of a radar is too much higher than that of wireless communications Tx, it is still higher than an LTE eNodeB's signal at a UE, even with a 50 MHz or 100 MHz offset. This implies that we must take into account interference caused by radars' out-of-band emissions when we analyze coexistence between a pulsed radar and a wireless communications system. As mentioned earlier, a

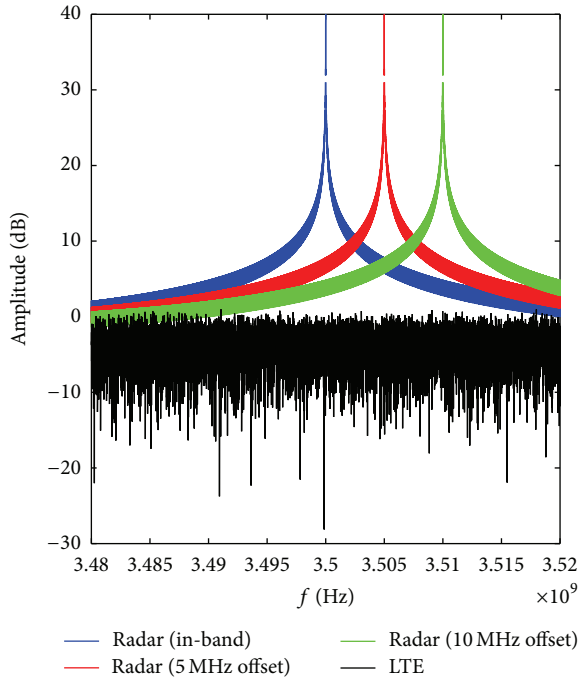

Figure 2: Impact of out-of-band emissions.

radar's out-of-band transmission does not cause significant interference to another radar in an adjacent band because transmitting powers of the radars are similar. However, to an LTE system, an out-of-band radar emission causes significant interference due to a significant difference in transmitting power between an LTE eNodeB and a radar.

Regarding the simulation setting discussed above, it is noteworthy to elaborate the rationale behind selection of the value of *path loss exponent* that equals 2. In the geography of the coexistence model, the lengths are significantly different between the two main parts: (i) between a radar and an LTE system and (ii) between an eNodeB and a UE in an LTE system. The idea is that the former part is much longer in distance and thus more affected by the path loss. In the former part of a coexistence geography, the path loss becomes the dominant channel impairment due to the long distance (e.g., tens of kilometers). On the other hand, in the latter part, radar interference becomes the main channel impairment since the path loss does not influence the performance due to short-distance propagation. As mentioned earlier, in a LTE-radar coexistence scenario, the former part is much longer in length than the latter part. Therefore, when selecting a value of the path loss exponent, it is the former part that we should consider more significantly than the latter part. Since the former part is very likely composed of a long line-of-sight path, it is approximated as 2 to give a conservative estimate, e.g., one that is less favorable to the LTE link.

Such interference from out-of-band radars can be interpreted as a greater number of radars that cause interference since radars operating in neighboring channels also cause interference to an OFDM system. Hence, there are additional bursts of interference from the out-of-band radars within an in-band radar's rotation period. It is likely that the radars have different values of T_{rot}, duty cycle, and PRT, which makes the task of an LTE system to track interfering pulses more difficult. In this paper we reflect the impact of out-of-band interference due to radars on lower and upper adjacent frequencies in such a way that there occurs a *threefold increase* in the number of OFDM symbols that are hit by a radar pulse. Therefore, *the total length of time that a radar interferes with an LTE cell within a radar rotation* T'_{intf}, can be given by $T'_{\text{intf}} \leq 3T_{\text{intf}}$. Note that $T'_{\text{intf}} = 3T_{\text{intf}}$ is true when there is no overlap in time among pulses generated by the three radars.

Table 2: Computation of the total interference time T'_{intf}.

θ_{beam} (deg)	θ_{intf} (deg)	T_{intf} (msec)	T'_{intf} (msec)
5	10.7	59.6	178.8
10	15.7	87.4	262.2
30	35.7	198.5	595.5

Table 2 demonstrates T'_{intf} according to different values of θ_{beam}, assuming that $T'_{\text{intf}} = 3T_{\text{intf}}$. We set θ_{beam} to 5, 10, and 30 degrees. Let us apply $T'_{\text{intf}} = 595.5$ msec to the current LTE standard as an example. Within a radar rotation time $T_{\text{rot}} = 2$ sec, 2000 LTE subframes can be transmitted. Since 14 OFDM symbols are transmitted in a subframe, 28000 OFDM symbols can be transmitted. As a result, $(595.5/2000) \times 28000 \approx 8337$ out of 28000 OFDM symbols are hit within a rotation of a radar.

3.2. Generalized Expression of Radar Interference. In the 3.5 GHz Band, radars report their operating parameters (i.e., pulse parameters and position) to a SAS, and an ESC also senses and sends the parameters to a SAS. Based on such a coexistence model, *the frequency of pulse interference within a certain time* can be quantified for use in analysis. There are four factors affecting the frequency: (i) the number of radars, (ii) PRT of a radar, (iii) level of interference from antenna sidelobes of a radar, and (iv) level of interference caused by out-of-band radars. However, it is extremely difficult for an ESC to keep track of all the four factors since military radars keep changing their parameters and the radars' parameters are even classified in many cases, as explained in an army's regulation document [22]. To this end, this paper generalizes the frequency of pulse occurrence by defining a quantity called *the probability of pulsed interference*, ρ. It is defined to be the probability that an OFDM system experiences a pulsed interference within a certain period of time. In this way, the quantity ρ generalizes the impacts of all of the four factors described above.

Note that this paper adopts the LTE standard's parameters for simulating a CBRS system as will be demonstrated in Section 6, and the scope of defining ρ is 1 msec, the length of a subframe defined in the LTE standard. If $\rho = 0$ during a simulation of 1000 subframes, none of the subframes are hit by a radar pulse. If $\rho = 1$, on the other hand, every subframe experiences radar interference during the simulation. Note that this analytical framework can be extended to any other type of OFDM communication without loss of generality. In other words, the definition of ρ can be set within any specified

Table 3: Existing ICI self-cancellation (ISC) schemes and the proposed subcarrier nulling ($L = 2$).

ICI self-cancellation (ISC) scheme	Subcarrier allocation
Data conversion [17]	$X'(k) = X(k), X'(k+1) = -X(k)$, where k is the subcarrier index
Symmetric data conversion	$X'(k) = X(k), X'(N-k-1) = -X(k)$, where N is the FFT size
Weighted data conversion [18]	$X'(k) = X(k), X'(k+1) = -\mu X(k)$, where μ is a real number in $[0, 1]$
Plural weighted data conversion [19]	$X'(k) = X(k), X'(k+1) = -e^{-j\pi/2}X(k)$
Data conjugate	$X'(k) = X(k), X'(k+1) = -X^*(k)$
Data rotated and conjugate [20]	$X'(k) = X(k), X'(k+1) = -e^{-j\pi/2}X^*(k)$
PSUN	$X'(k) = X(k), X'(k+1) = 0$

time period that can be measured by the number of OFDM symbols.

4. Precoded SUbcarrier Nulling (PSUN)

4.1. Proposition of PSUN. Pulse blanking (PB) is known to be one of the most effective techniques for suppressing pulsed interference [23–25]. Unfortunately, PB still leaves a significant level of ICI. In PB, time domain samples of the received signal affected by pulsed interference are set to zero. The technique deteriorates performance of an OFDM system by affecting not only the interfered samples but also the desired samples. This problem occurs due to the fact that (inverse) Fourier transform provides a time-frequency mapping in such a way that every frequency/time sample contributes to generating a time/frequency symbol. In an OFDM system, PB takes place in the time domain whereas the data symbols are mapped to the subcarriers in the frequency domain. An OFDM Rx blanks only several samples that are radar-interfered in the time domain. However, such a partial change leads to corruption of all the samples in the frequency domain due to characteristic of the Fourier transform, which still causes ICI. This paper focuses on suppression of such ICI that remains after applying PB at an OFDM Rx.

This paper suggests that the negative impact of PB can be considered a form of time-selective fading. Channel coding is usually applied in combination with interleaving and diversity to mitigate performance degradation due to fading [26]. In OFDM systems, the main means of combating time-selective fading are block interleaving and antenna diversity. However, our results indicate that neither method can effectively mitigate ICI caused by PB. Interleaving is ineffective because PB does not result in bursty errors due to the one-to-all mapping characteristic of the Fourier transform. Antenna diversity is also not effective against the ICI caused by PB because an entire LTE cell is likely to be hit at once by a radar's beam. A multiple-antenna technology can bring no benefit when the signals received by all the antennas are interfered with simultaneously.

ICI self-cancellation (ISC) is an aggressive means of combating ICI. It cancels ICI by allocating precoded $L-1$ redundant subcarriers between data subcarriers, which results in a $1/L$ data rate. Based on the work of Zhao and Haggman [17], several ISC schemes have been proposed [18–20]. Some of the existing ISC schemes are summarized in Table 3, assuming $L = 2$. Note that $X(\cdot)$ and $X'(\cdot)$ indicate the original transmitted data symbol and the symbol after ISC precoding, respectively.

We discovered that the most effective way of reducing ICI induced by PB is *to insert null subcarriers*, instead of allocating any other types of redundant subcarriers. The rationale is illustrated in Figure 3. It is an example that is simplified to clearly demonstrate the impact of location of PB on the level of ICI. Figure 3(a) represents an example signal at Tx while Figures 3(b) and 3(c) show *two different locations of PB* at Rx. The example signal contains three among 64 subcarriers around the center (28th, 30th, and 32nd) that are set to 1 while all the others are set to 0. Note that the transmitted signal in Figure 3(a) shows the real part of the original complex signal. It is observed from Figure 3 that the location of PB has a very significant impact on the level of ICI caused by PB. Comparing Figures 3(b) and 3(c), *the ICI becomes more severe as higher-amplitude samples are blanked*. In other words, the ICI level can be reduced as the time domain fluctuation gets flatter. It is straightforward that the simplest way of keeping time domain amplitudes low is to reduce the number of subcarriers. An OFDM Rx can suppress ICI remaining after PB better when a Tx has allocated *null subcarriers* instead of other types of redundancy, since use of null subcarriers reduces the number of high-energy bins in the time domain.

For this reason, an OFDM Tx employing PSUN *precodes an OFDM symbol by inserting null tones between data tones so that the ICI after PB at its Rx can be suppressed*. This makes PSUN a type of ISC, as listed in Table 3. Various manners of inserting null tones for different purposes have been studied in the literature [27–29]. In this work, PSUN allocates the null tones in such a way that the radar interference is minimized. Figure 4 shows that PSUN outperforms the other ISC schemes. Note that for the weighted data conversion scheme the value of μ becomes $1/2$. The reason for PSUN's higher performance is that PSUN yields smaller variation of an OFDM symbol in the time domain because it transmits a smaller number of subcarriers.

4.2. The Transmission Protocol of PSUN. Let r denote the coding rate of PSUN. With the coding rate of $r = 1/L$, PSUN inserts $L-1$ null tones between data tones. Figure 5 illustrates how PSUN inserts null tones in an exemplar OFDM symbol, with QPSK and the FFT size of 32. Figure 5(a) demonstrates an OFDM symbol without PSUN. Figures 5(b) and 5(c) show

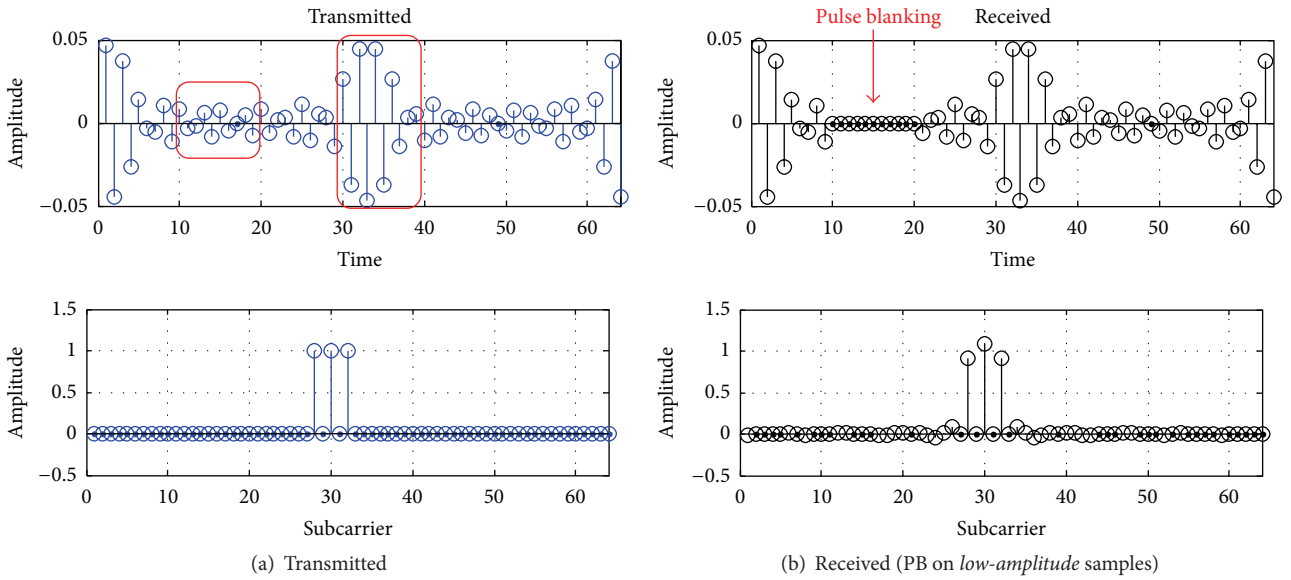

(a) Transmitted

(b) Received (PB on *low-amplitude* samples)

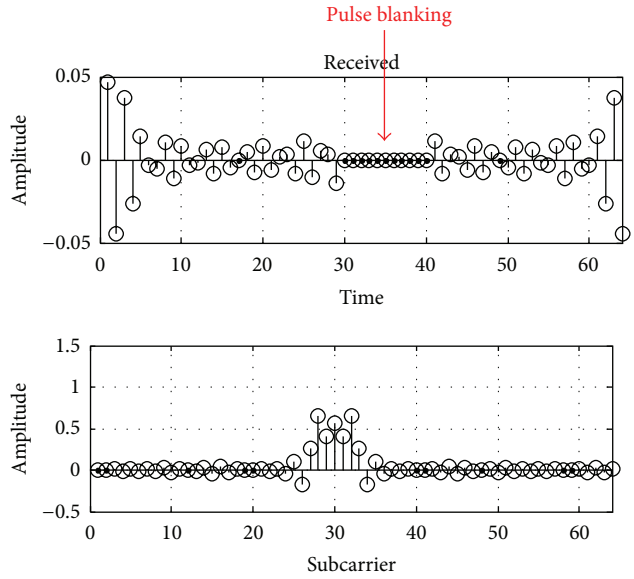

(c) Received (PB on *high-amplitude* samples)

FIGURE 3: Dependency of ICI on the location of PB.

examples of precoding the OFDM symbol using PSUN with r equal to 1/2 and 1/4, respectively. PSUN extracts the first half/fourth of the data tones from the original OFDM symbol given in Figure 5(a). Note that this method of taking $1/L$ of its original data is only an example. PSUN can do it in various other ways; another example is to extract a data tone in every L subcarrier. Then PSUN inserts null tones (marked with red squares) between the data tones, which leads to the mapping illustrated in Figures 5(b) and 5(c).

This is where PSUN sacrifices data rate by $1/r$ within an OFDM symbol. To minimize such loss of data rate, an OFDM Tx performs two important operations when adopting PSUN. First, it *localizes OFDM symbols to be hit a priori and allocates null tones in the symbols only*. The a priori knowledge about radar pulse parameters is provided by a SAS but sensed by an ESC beforehand. Figure 6 shows a subframe in which an OFDM symbol is expected to be hit by a radar pulse. Only that symbol is precoded with the null subcarriers at Tx before transmission. Second, within the OFDM symbol to be radar-interfered, an OFDM Tx *disables channel coding and shifts the saved redundancy to PSUN*. This assumes that, for an OFDM symbol to be radar-interfered, the pulsed interference is more severe than AWGN. This protects the symbol from radar interference, while keeping the total number of transmitted bits the same. Multiple OFDM symbols can be hit simultaneously because an interference pulse can be either shorter or longer than an OFDM symbol. In this case, the OFDM symbols are all precoded. All the other symbols that are not precoded are transmitted with channel coding and full data tones.

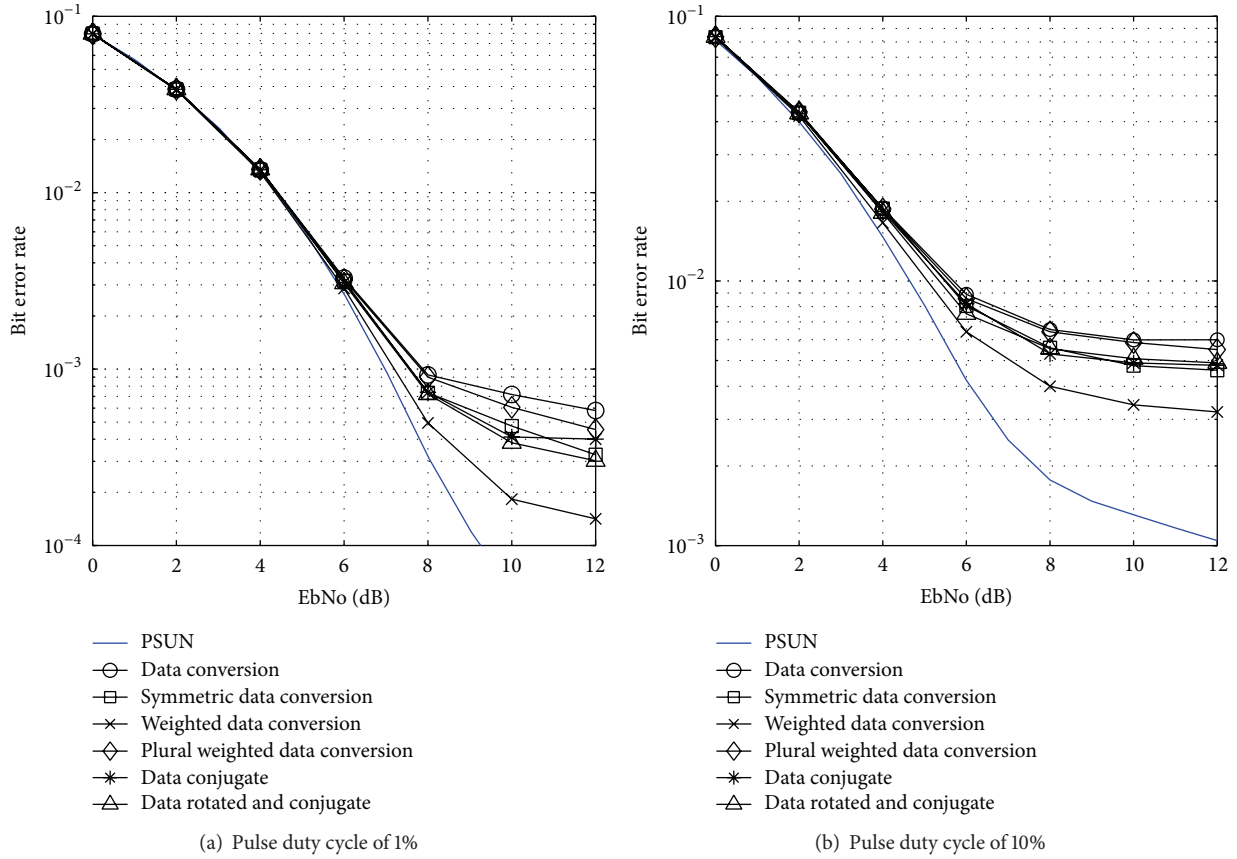

(a) Pulse duty cycle of 1%

(b) Pulse duty cycle of 10%

Figure 4: Comparison of PSUN to other ISC schemes (QPSK, 1024-FFT).

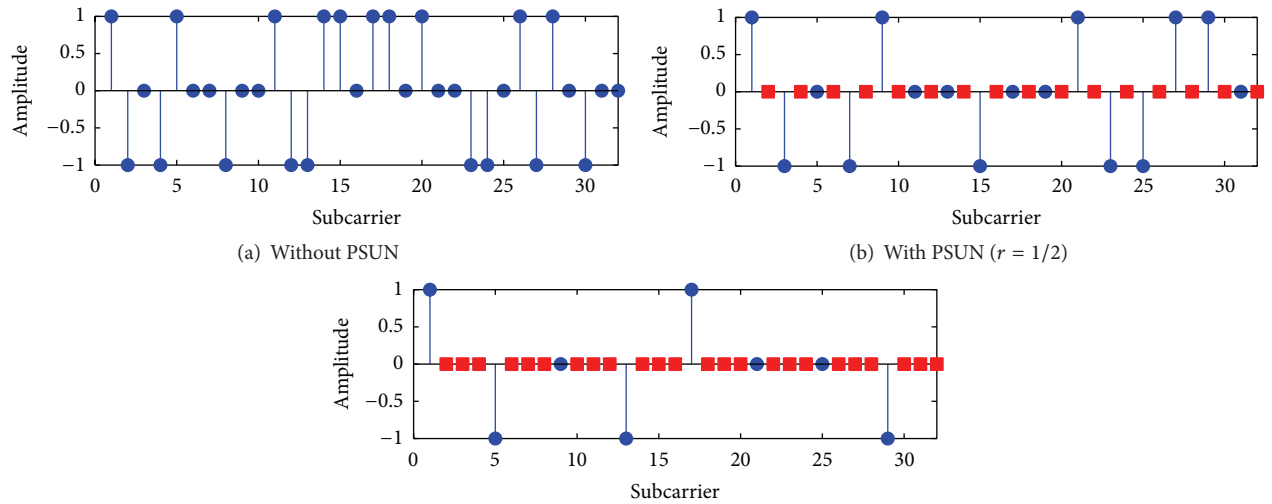

(a) Without PSUN

(b) With PSUN ($r = 1/2$)

(c) With PSUN ($r = 1/4$)

Figure 5: An OFDM symbol applying PSUN (QPSK, 32-FFT).

Figure 6 illustrates PSUN from such a macroscopic standpoint. An OFDM Tx employing PSUN reduces loss of data rate by *selecting certain OFDM symbols to insert null subcarriers*. According to the FCC's suggestion, a priori knowledge of interference from incumbent radars is available at an LTE eNodeB. Radars report their operating parameters (i.e., pulse parameters and position) to a SAS, and an ESC also senses the parameters and sends them to a SAS.

Taking LTE as an example of a CBRS system, there are 14 OFDM symbols in a subframe. Figure 5 showed only

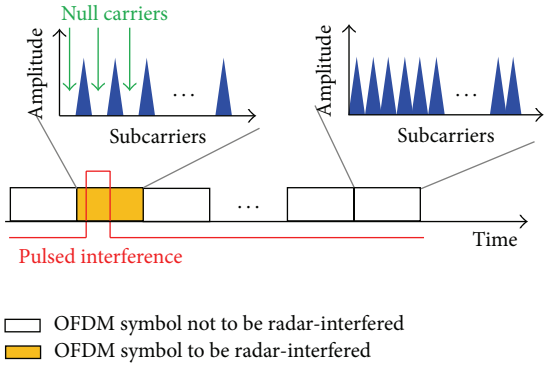

FIGURE 6: Transmission protocol of PSUN ($r = 1/2$).

one OFDM symbol that is expected to be hit by a radar pulse. In Figure 6, an OFDM symbol to be radar-interfered is highlighted by orange color. However, there are 13 other OFDM symbols that are not radar-interfered. An OFDM Tx applying PSUN does not precode these OFDM symbols for two reasons: (i) they undergo AWGN channels against which channel coding achieves better protection than PSUN; (ii) thus, as explained earlier, unnecessary loss of data rate can be avoided by not applying redundancy in subcarriers.

It is possible that two or more consecutive OFDM symbols can be interfered by the same pulse because an interference pulse can be either shorter or longer than an OFDM symbol depending on the pulse's duty cycle. In such a case, all of the OFDM symbols that are expected to be radar-interfered are precoded.

5. Imperfect Pulse Prediction

We discovered that three types of imperfect pulse prediction are possible in a 3.5 GHz band coexistence framework: (i) false prediction; (ii) missed prediction; and (iii) mislocation. *False alarm* and *missed detection* are defined as an ESC's inaccurate claim of presence/absence of an interfering radar pulse, given that a pulse is in fact absent/present. *Mislocation* is a unique type of imperfect pulse prediction that we suggest in this paper. It occurs when an ESC accurately predicts the location of a pulse interference in terms of *subframe* but being inaccurate in terms of *symbol* within a subframe. More specifically, it is called a mislocation when an ESC predicts that an OFDM symbol within a subframe will be hit by a radar pulse and in fact the interference actually occurs at the predicted subframe but at a different OFDM symbol.

Let us interpret actual impacts of the three types of imperfect pulse prediction. Recall that channel coding and PSUN are countermeasures against AWGN and pulsed interference, respectively. A *false alarm* is interpreted as a situation where an OFDM symbol that is not to be radar-interfered is predicted to be radar-interfered and thus precoded with PSUN. Therefore, in the OFDM symbol, redundant bits for channel coding are removed and null subcarriers are allocated instead which is a weaker protection than channel coding against AWGN, but in fact the symbol is not hit by a radar pulse but goes through an AWGN channel. On the other hand, when a *missed detection* occurs, an OFDM symbol to be radar-interfered is not predicted to be radar-interfered and thus not precoded with PSUN. Thus the OFDM symbol is protected with channel coding instead which is a weaker protection than PSUN against pulsed interference. Overall, although in the opposite way, either a false alarm or missed detection deteriorates performance of an OFDM system that applies PSUN. Most interestingly, a *mislocation* has the impact of a false alarm and missed detection within a single subframe. Recall that a false alarm unnecessarily precodes an OFDM symbol that will undergo AWGN with PSUN, while missed detection does not precode a symbol that will be hit by a radar pulse. Let us assume that an ESC has predicted an OFDM symbol named "A" to be hit by a radar pulse and hence has precoded it. A mislocation occurs when in fact another OFDM symbol called "B" has actually been hit. The problem is that OFDM symbol "B" has not been precoded with null subcarriers since the ESC has predicted it not to be hit by a radar pulse but to go through an AWGN channel. Therefore, a mislocation results in two OFDM symbols that are incorrectly precoded within a single subframe. OFDM symbol "A" has been protected against a radar pulse but has actually undergone an AWGN, while "B" has been believed to experience an AWGN and thus has not been precoded but in fact has gone through a radar interference. To interpret this situation, a false alarm has occurred at OFDM symbol "A" whereas missed detection has happened at "B." This is how a mislocation causes a false alarm and missed detection at the same time within one subframe.

Major causes of the above imperfect pulse prediction are twofold. Firstly, an ESC can cause sensing errors. Secondly, an ESC can lose track of radars' pulse parameters. The former affects false alarm and missed detection, while the latter impacts all of the three types of imperfect pulse prediction.

5.1. Sensing Error by an ESC. Typically for a protocol requiring spectrum sensing, either a matched filter or an energy detector can be used [30, 31]. This paper assumes that an ESC, a device with sensing capability, uses an energy detector. Assuming that an interference signal from a radar and noise are both modeled as white Gaussian processes, the problem of sensing a radar's pulsed interference signal by an ESC can be given by the following hypotheses test:

$$\begin{aligned} H_0&: Y \sim \mathcal{N}\left(0, \sigma_0^2\right), \\ H_1&: Y \sim \mathcal{N}\left(0, \sigma_0^2 + \sigma_1^2\right), \end{aligned} \tag{4}$$

where

Y is an observation sample;

σ_0^2 is power of noise;

σ_1^2 is power of an interference signal.

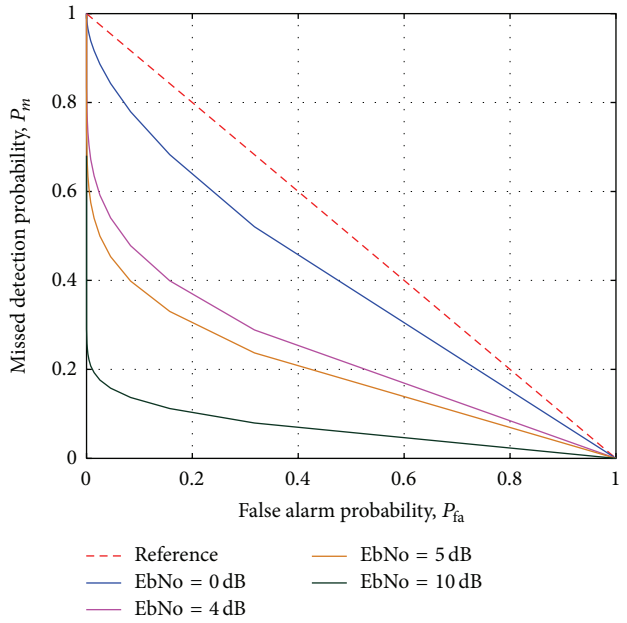

Figure 7: ROCs of the energy detector at an ESC.

Since an ESC adopts an energy detector, based on the Neyman-Pearson detection theory, the probability of false alarm, P_{fa}, and missed detection, P_m, are defined by

$$P_{\text{fa}} \triangleq \Pr\left(H_1 \mid H_0\right) = 1 - \Gamma\left(\frac{1}{2}, \frac{\eta_{\text{se}}}{2\sigma_0^2}\right),$$
$$P_m \triangleq \Pr\left(H_0 \mid H_1\right) = 1 - \Gamma\left(\frac{1}{2}, \frac{\eta_{\text{se}}}{2\left(\sigma_0^2 + \sigma_1^2\right)}\right), \tag{5}$$

where η_{se} denotes the sensing error threshold and the incomplete gamma function is given by

$$\Gamma(t, z) = \frac{1}{\Gamma(t)} \int_0^x t^{t-1} e^{-x} dx. \tag{6}$$

A receiver operating characteristic (ROC) curve is used for an analysis of interplay between P_{fa} and P_m. Figure 7 shows ROCs of (5) according to the energy per bit to noise power spectral density ratio (EbNo). An increase in the sensing threshold for given signal and noise power values moves the operating point toward the upper direction along one of the curves in the figure. At a high EbNo regime both P_m and P_{fa} can maintain low values, even if the sensing threshold changes much. This is not the case for low EbNo.

5.2. Loss of Track of Radars' Operating Information. It is difficult to track a radar's pulsed signals for the following two reasons. Firstly, the pulse information might not be fully available to the SAS. There has been strong opposition from military stakeholders to provide information to the database about radars' position or other information that could make them more prone to be affected by enemy jammers. Secondly, a radar may change its pulse parameters and position for various purposes, such as higher security or avoidance of interference among radars. According to a recent extensive survey paper [32], most radar systems have fixed position and operating parameters. However, airborne and shipborne radars may not have preplanned routes and, therefore, an error region has to be defined for such cases. In this case, there occurs a time during which an ESC loses track of a radar's pulse parameters. An ESC requires some time to sense a radar's parameter changes, during which it cannot avoid providing outdated information to a SAS.

We suggest that an ESC's losing track of radars' operating information must be understood more seriously than an ESC's sensing errors. The reason is that it is more likely and can cause any of the three types of imperfect pulse prediction but is more difficult to study since it is not a characteristic of an ESC but that of a radar which is an independent variable in this paper. Therefore, this paper provides a framework for analyzing this loss of track. Values of the false alarm, missed detection, and mislocation probabilities, P_{fa}, P_m, and P_{ml}, over the interval of [0,1] are considered, so that the analysis can be generalized over any case in which an ESC loses track of radars' operating parameters.

6. Performance Evaluation

6.1. Simulation Setup. The discussion in [9, 10] can be interpreted that the CBRS system coexisting with the pulse radar utilizes spectrum more efficiently in the downlink than in the uplink, in terms of the data rate per megahertz. Hence, spectrum sharing with radar would be more appropriate for applications that require greater capacity in the downlink than the uplink, which is a typical characteristic of many applications. Therefore, this paper assesses the performance of the downlink of an LTE system by measuring *the number of bits per second that an LTE UE successfully receives*. The number of *transmitted* bits differs according to the modulation scheme. (In this paper's simulations 16-QAM and 64-QAM were evaluated.) We analyze the metric as functions of six variables that are chosen to represent three different aspects of coexistence between an LTE Rx and military radars as follows. (i) EbNo represents impact of AWGN; (ii) pulse duty cycle and ρ represent characteristics of interference by a radar; (iii) P_{fa}, P_m, and P_{ml} represent impacts of imperfect pulse prediction. Each variable gauges different levels of channel impairment, that is, AWGN or radar interference. It differentiates the bit error rates which again directly determines the number of *received* bits.

Table 4 summarizes the simulation parameters for LTE and radar. We leverage LTE physical-layer simulations which are 3GPP compliant [33]. The FFT size is set to 1024 but the results based on this parameter can hold for other values of FFT size. The reason is that PB is a channel impairment that occurs in time domain, and LTE is always synchronized in time regardless of FFT size. Coding rates of channel coding and PSUN are kept identical to be $r = 1/2$, for ease of demonstrating the impacts of shifting redundancy from channel coding to subcarrier nulling. The only two channel impairments that are considered in this paper are AWGN and radar interference; as a result no typical fading effects are considered. Hence the simulations do not accurately follow

Table 4: Simulation parameters.

Parameter	Value
LTE	
FFT size	1024
Subcarrier spacing	15 kHz
Sampling frequency	15.36 MHz
OFDM symbol time	66.7 μs
Subframe length	1 ms
CP length	5.2 μs (1st)/4.69 μs (the following 6)
OFDM symbols/subframe	14
Modulation	16-QAM, 64-QAM
Channel coding	(133,171) convolutional code ($r = 1/2$)
PSUN	$r = 1/2$
Radar	
Pulse repetition time	1 ms
Rotation rate	30 rpm

the modulation and coding scheme (MCS) that are associated with channel quality indicator (CQI). *In order for LTE to operate in the 3.5 GHz band, a new set of MCS and CQI must be matched.* Radar pulse repetition time is set identical to an LTE subframe duration (1 msec) for accuracy of computation. Each simulation is conducted through 10^6 subframes.

To elaborate the discussion about a new set of MCS and CQI, we claim that it will be necessary because the 3.5 GHz environment is a totally different one from the previous spectrum bands in which LTE systems have been operating. In addition to all the mobility and multipath impacts, design of an LTE system at the 3.5 GHz band needs to consider pulsed interference generated by radars. However, this exceeds the scope of this paper and will be discussed in our future work. In other words, the results that are discussed in this paper do not have any impact from the new set of MCS and CQI.

6.2. Results

6.2.1. EbNo. Figure 8(a) shows the number of received bits per second versus EbNo with 16-QAM and 64-QAM. Recall that an OFDM Tx employing PSUN disables channel coding but puts the redundancy saved from no channel coding to null subcarriers between data subcarriers instead. In low EbNo region, AWGN is the predominating channel impairment that outweighs radar interference, which results in lower effectiveness of PSUN. In other words, outperformance of PSUN over the case without PSUN gets increased as EbNo gets higher. In that way, radar interference becomes prevailing which leads to greater performance advantage of PSUN. Moreover, such advantage of PSUN gets greater with higher modulation order.

6.2.2. Pulse Parameters of the Radar. Figure 8(b) demonstrates the number of received bits per second versus the duty cycle of a radar pulse. We generalized the values of pulse duty cycle for wider generality of this work, although many of the pulsed radars deployed in practice use relatively small values of duty cycle, for example, 0.1–10%. It is straightforward that higher pulse duty cycle yields greater outperformance of PSUN over the case without PSUN. Also, similar to the results with EbNo above, performance advantage gets greater as the modulation order becomes higher.

Figure 8(c) illustrates the number of received bits per second versus the probability that an OFDM symbol is hit by a radar pulse, ρ. When $\rho = 0$, the performance must be the same between the cases with and without PSUN since PSUN does not allocate null subcarriers when no OFDM symbol is radar-interfered. As explained in Section 3.2, a greater value of ρ yields a smaller number of received bits per second. Similar to the discussion of pulse duty cycle in Figure 8(b), a greater value of ρ indicates a more severe situation of radar interference. Due to this, it still holds true that outperformance of PSUN increases as ρ becomes greater. The performance curve drops faster in 64-QAM than 16-QAM, which implies that higher-order modulation is more sensitive to radar interference. Nevertheless, performance advantage of PSUN gets greater as the modulation order gets higher.

6.2.3. Pulse Prediction Errors. So far we have seen the performances assuming *perfect pulse prediction*. The results shown through Figures 8(d) and 8(f) depict how the performance of an OFDM system is deteriorated with *imperfect pulse prediction*. Figure 8(d) shows the number of received bits per second versus the probability of false alarm, P_{fa}. It is straightforward that higher P_{fa} decreases the number of received bits per second of an OFDM system employing PSUN, while the case without PSUN stays unrelated to the level of P_{fa}. The reason is that, with a false alarm, an OFDM symbol is protected by PSUN instead of channel coding, but in fact it undergoes an AWGN channel where channel coding is more effective protection than PSUN.

Figure 8(e) shows the number of received bits per second versus the probability of missed detection, P_m. As explained earlier in Section 5, at an OFDM Tx applying PSUN, missed detection is translated as a situation where an OFDM symbol is not predicted to be radar-interfered and hence not precoded with PSUN but in fact hit by a radar pulse. In other words, the particular symbol is equipped with channel coding instead of PSUN and hence contributes to degradation of performance. The performance degradation of OFDM Rx without PSUN is shown by the gap at zero P_m. As P_m increases, the performance of PSUN gets closer to the case without PSUN. The performance advantage of PSUN increases as the modulation order gets higher.

Figure 8(f) shows the number of received bits per second versus the probability of pulse mislocation, P_{ml}. A mislocation refers to a wrong location of to-be-interfered OFDM symbol within a subframe. Recall that, with a mislocation, a false alarm and missed detection occur at the same time within a subframe. This is why performance propensity according to P_{ml} from Figure 8(f) is nearly linear while the ones according to P_{fa} and P_m are logarithmic and exponential, respectively, as observed from Figures 8(d) and 8(e).

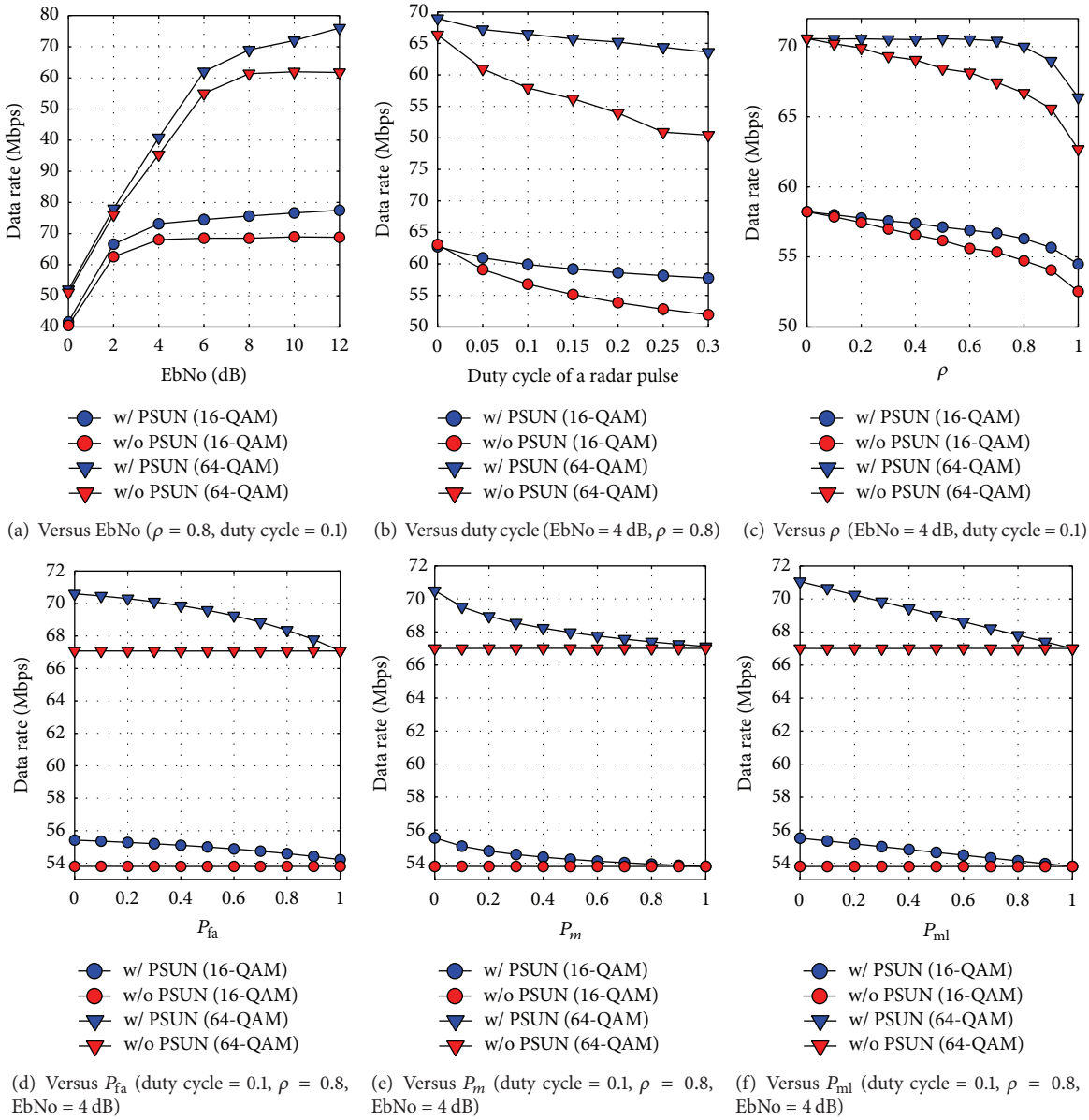

(a) Versus EbNo (ρ = 0.8, duty cycle = 0.1)

(b) Versus duty cycle (EbNo = 4 dB, ρ = 0.8)

(c) Versus ρ (EbNo = 4 dB, duty cycle = 0.1)

(d) Versus P_{fa} (duty cycle = 0.1, ρ = 0.8, EbNo = 4 dB)

(e) Versus P_m (duty cycle = 0.1, ρ = 0.8, EbNo = 4 dB)

(f) Versus P_{ml} (duty cycle = 0.1, ρ = 0.8, EbNo = 4 dB)

Figure 8: Data rate versus EbNo, the duty cycle of a radar pulse, ρ, P_{fa}, P_m, and P_{ml}.

7. Feasibility of 5G Applications Using 3.5 GHz LTE with PSUN

Fifth-generation (5G) mobile networks will operate in a highly heterogeneous environment characterized by the existence of multiple types of access technologies over multiple chunks of spectrum bands. In other words, enabling 5G use cases and business models requires the allocation of additional spectrum for mobile broadband and needs to be supported by flexible spectrum management capabilities. Based on the analyses and results of this paper, we suggest that the 3.5 GHz band can be a usable additional spectrum for enabling LTE to support several functionalities of 5G technologies.

We refer to a white paper [21] issued by the Next Generation Mobile Networks (NGMN), a mobile telecommunications association of mobile operators, vendors, manufacturers, and research institutes, for understanding the representative example use cases of 5G and the corresponding requirement of data rate for each use case. A consistent user experience with respect to throughput needs a minimum data rate guaranteed everywhere. The data rate requirement of a use case is set as the minimum user experienced data rate required for the user to have a quality experience of the targeted use case. The use cases are summarized in Table 5.

According to our results, LTE with PSUN can fulfill the *downlink* requirements of several use cases which are listed under the category of "candidates for LTE with PSUN" in

Table 5: Data rate requirements for use cases of 5G [21].

Use case	Data rate requirement (downlink/uplink)
Candidates for LTE with PSUN	
Massive low-cost/long-range/low-power M2M	1–100 kbps
Resilience and traffic surge	0.1–1 Mbps/0.1–1 Mbps
Ultrahigh reliability & ultralow latency	50 kbps to 10 Mbps/a few kbps to 10 Mbps
Ultrahigh availability & reliability	10 Mbps/10 Mbps
Airplanes connectivity	15 Mbps/7.5 Mbps
Broadband access in a crowd	25 Mbps/50 Mbps
50+ Mbps everywhere	50 Mbps/25 Mbps
Ultralow latency	50 Mbps/25 Mbps
Others	
Broadband like services	Up to 200 Mbps/modest (e.g., 500 kbps)
Ultralow-cost broadband access	300 Mbps/50 Mbps
Mobile broadband in vehicles	300 Mbps/50 Mbps
Broadband access in dense areas	300 Mbps/50 Mbps
Indoor ultrahigh broadband access	1 Gbps/500 Mbps

Table 5. While most of the requirements of the selected use cases are set to be 50 Mbps, our results (Figures 8(a) through 8(f)) indicate that LTE with PSUN is capable of supporting data rates that are higher than 50 Mbps and 40 Mbps with 64-QAM and 16-QAM, respectively. For example, observing Figure 8(a), the required EbNo values for achieving the data rate of 50 Mbps are 0 and 1 dB for 64-QAM and 16-QAM, respectively.

It is discussed in [9, 10] that although average data rate is roughly the same for all file sizes, because of interruptions as a radar rotates, average received data rate for smaller files may vary depending on when the transmission begins relative to the radar's rotation cycle. This effect does not occur during transmission of larger files that span one or more rotation periods of the radar. The authors suggested several appropriate applications that can tolerate interruptions from a pulsed radar, video on demand, peer-to-peer file sharing, and automatic meter reading, or applications that transfer large enough files so the fluctuations are not noticeable, such as song transfers. Among these applications, a white paper that analyzed the mobile traffic pattern of 2015 [34] finds a direction that LTE with PSUN can target in the 3.5 GHz band. It says that *mobile video traffic* accounted for 55% of total mobile data traffic in 2015. Mobile video traffic now accounts for more than half of all mobile data traffic. It will be very promising if LTE with PSUN can support video traffic in the 3.5 GHz band while coexisting with military radar.

8. Conclusion

This paper proposes PSUN, an OFDM transmission scheme enabling an LTE system to coexist with federal military radars in the 3.5 GHz band. The scheme is comprised of PB at an Rx and precoding of null subcarriers at Tx of an OFDM system. To maximize data rate, OFDM Tx employing PSUN (i) localizes OFDM symbols to be radar-interfered a priori and (ii) shifts redundancy from channel coding to subcarriers in the OFDM symbols. This paper considers existence of sensing functionality in the 3.5 GHz band coexistence architecture and hence impacts of imperfect sensing which can occur due to a sensing error by ESC and parameter changes by a radar. Results show that PSUN is still effective in suppressing ICI remaining after PB even with imperfect pulse prediction and as a result enables an LTE system to support various use cases of 5G that require the data rate lower than 50 Mbps in the downlink and relatively larger file size such as video streaming.

Disclosure

This work was presented, in part, in the 2nd IEEE WCNC International Workshop on Smart Spectrum Technologies (IWSS 2016), Doha, Qatar, on 3 April 2016.

Competing Interests

The authors declare that they have no competing interests.

References

[1] NTIA, *An Assessment of the Near-Term Viability of Accommodating Wireless Broadband Systems in the 1675–1710 MHz, 1755–1780 MHz, 3500–3650 MHz, 4200–4220 MHz and 4380–4400 MHz Bands*, NTIA, 2010.

[2] Memorandum for the Heads of Executive Departments and Agencies, *Unleashing the Wireless Broadband Revolution*, 2010.

[3] FCC 12-148, "Amendment of the commision's rules with regard to commercial operations in the 3550–3650 MHz band," Notice of Proposed Rulemaking in GN Docket 12-354, 2012.

[4] FCC 14-49, "Amendment of the commission's rules with regard to commercial operations in the 3550–3650 MHz band," Further Notice of Proposed Rulemaking in GN Docket 12-354, 2015.

[5] FCC 15-47, "Amendment of the commissions rules with regard to commercial operations in the 3550–3650 MHz band," Report and Order and Second Further Notice of Proposed Rulemaking in GN Docket 12-354, 2015.

[6] NTIA, "Response to commercial operations in the 3550–3650 MHz band," GN Docket 12-354, 2015.

[7] S. Sodagari, A. Khawar, T. C. Clancy, and R. McGwier, "A projection based approach for radar and telecommunication systems coexistence," in *Proceedings of the IEEE Global Communications Conference (GLOBECOM '12)*, pp. 5010–5014, Anaheim, Calif, USA, December 2012.

[8] A. Khawar, A. Abdel-Hadi, and T. C. Clancy, "Spectrum sharing between S-band radar and LTE cellular system: a spatial approach," in *Proceedings of the IEEE International Symposium on Dynamic Spectrum Access Networks (DYSPAN '14)*, pp. 7–14, McLean, Va, USA, April 2014.

[9] R. Saruthirathanaworakun, J. M. Peha, and L. M. Correia, "Opportunistic sharing between rotating radar and cellular," *IEEE Journal on Selected Areas in Communications*, vol. 30, no. 10, pp. 1900–1910, 2012.

[10] R. Saruthirathanaworakun, J. M. Peha, and L. M. Correia, "Gray-space spectrum sharing between multiple rotating radars and cellular network hotspots," in *Proceedings of the IEEE 77th Vehicular Technology Conference (VTC '13)*, June 2013.

[11] F. Paisana, J. P. Miranda, N. Marchetti, and L. A. DaSilva, "Database-aided sensing for radar bands," in *Proceedings of the IEEE International Symposium on Dynamic Spectrum Access Networks (DYSPAN '14)*, pp. 1–6, McLean, Va, USA, April 2014.

[12] M. Ghorbanzadeh, E. Visotsky, P. Moorut, W. Yang, and C. Clancy, "Radar in-band interference effects on macrocell LTE uplink deployments in the U.S. 3.5 GHz band," in *Proceedings of the International Conference on Computing, Networking and Communications (ICNC '15)*, pp. 248–254, Garden Grove, Calif, USA, February 2015.

[13] M. Ghorbanzadeh, E. Visotsky, P. Moorut, W. Yang, and C. Clancy, "Radar inband and out-of-band interference into LTE macro and small cell uplinks in the 3.5 GHz band," in *Proceedings of the IEEE Wireless Communications and Networking Conference (WCNC '15)*, pp. 1829–1834, March 2015.

[14] H.-A. Safavi-Naeini, C. Ghosh, E. Visotsky, R. Ratasuk, and S. Roy, "Impact and mitigation of narrow-band radar interference in down-link LTE," in *Proceedings of the IEEE International Conference on Communications (ICC '15)*, pp. 2644–2649, London, UK, June 2015.

[15] S. Kim, J. Choi, and C. Dietrich, "Coexistence between OFDM and pulsed radars in the 3.5 GHz band with imperfect sensing," in *Proceedings of the IEEE Wireless Communications and Networking Conference*, Doha, Qatar, April 2016.

[16] M. Cotton and R. Dalke, "Spectrum occupancy measurements of the 3550–3650 Megahertz maritime radar band near San Diego, California," NTIA Report TR-14-500, 2014.

[17] Y. Zhao and S.-G. Haggman, "Sensitivity to Doppler shift and carrier frequency errors in OFDM systems-the consequences and solutions," in *Proceedings of the IEEE 46th Vehicular Technology Conference*, vol. 3, pp. 1564–1568, Atlanta, Ga, USA, May 1996.

[18] Y. Fu and C. Ko, "A new ICI self-cancellation scheme for OFDM systems based on a generalized signal mapper," in *Proceedings of the 5th International Symposium on Wireless Personal Multimedia Communications*, vol. 3, pp. 995–999, IEEE, 2002.

[19] Y.-H. Peng, Y.-C. Kuo, G.-R. Lee, and J.-H. Wen, "Performance analysis of a new ICI-self-cancellation-scheme in OFDM systems," *IEEE Transactions on Consumer Electronics*, vol. 53, no. 4, pp. 1333–1338, 2007.

[20] Q. Shi, Y. Fang, and M. Wang, "A novel ICI self-cancellation scheme for OFDM systems," in *Proceedings of the 5th International Conference on Wireless Communications, Networking and Mobile Computing (WiCOM '09)*, pp. 1–4, IEEE, Beijing, China, September 2009.

[21] The Next Generation Mobile Networks, *NGMN 5G White Paper*, The Next Generation Mobile Networks Ltd., Frankfurt, Germany, 2015.

[22] Operations and SignalSecurity, Army Regulation 530-1, 2005.

[23] S. Brandes, *Suppression of Mutual Interference in OFDM Based Overlay Systems*, Universitat Fridericiana Karlsruhe, Karlsruhe, Germany, 2009.

[24] S. Brandes, U. Epple, and M. Schnell, "Compensation of the impact of interference mitigation by pulse blanking in OFDM systems," in *Proceedings of the IEEE Global Telecommunications Conference (GLOBECOM '09)*, pp. 1–6, Honolulu, Hawaii, USA, December 2009.

[25] U. Epple, D. Shutin, and M. Schnell, "Mitigation of impulsive frequency-selective interference in OFDM based systems," *IEEE Wireless Communications Letters*, vol. 1, no. 5, pp. 484–487, 2012.

[26] A. Goldsmith, *Wireless Communications*, Cambridge University, Cambridge, UK, 2005.

[27] S. Ahmed and M. Kawai, "Dynamic null-data subcarrier switching for OFDM PAPR reduction with low computational overhead," *Electronics Letters*, vol. 48, no. 9, pp. 498–499, 2012.

[28] M. Ghogho, A. Swami, and G. B. Giannakis, "Optimized null-subcarrier selection for CFO estimation in OFDM over frequency-selective fading channels," in *Proceedings of the IEEE Global Telecommunicatins Conference (GLOBECOM '01)*, pp. 202–206, San Antonio, Tex, USA, November 2001.

[29] B. Wang, P.-H. Ho, and C.-H. Lin, "OFDM PAPR reduction by shifting null subcarriers among data subcarriers," *IEEE Communications Letters*, vol. 16, no. 9, pp. 1377–1379, 2012.

[30] H. V. Poor, *An Introduction to Signal Detection and Estimation*, Springer, New York, NY, USA, 2nd edition, 1994.

[31] J. W. Chong, D. K. Sung, and Y. Sung, "Cross-layer performance analysis for CSMA/CA protocols: impact of imperfect sensing," *IEEE Transactions on Vehicular Technology*, vol. 59, no. 3, pp. 1100–1108, 2010.

[32] F. Paisana, N. Marchetti, and L. A. Dasilva, "Radar, TV and cellular bands: which spectrum access techniques for which bands?" *IEEE Communications Surveys and Tutorials*, vol. 16, no. 3, pp. 1193–1220, 2014.

[33] 3GPP, "Further advancements for EUTRA physical layer aspects, release 9," 3GPP TR 36.814 V9.0.0 (2010-03), 2010.

[34] Cisco, "Cisco visual networking index: global mobile data traffic forecast update," White Paper 20152020, 2016.